Tidal and meteorological forcing of sediment transport in tributary mudflat channels

David K. Ralston*

Department of Civil and Environmental Engineering,
University of California, Berkeley
Berkeley, CA

Mark T. Stacey

Department of Civil and Environmental Engineering
University of California, Berkeley
Berkeley, CA

Submitted to *Continental Shelf Research*, January 31, 2006
Accepted for publication January 11, 2007

*current contact information:
Applied Ocean Physics and Engineering
Woods Hole Oceanographic Institution, MS 12
Woods Hole, MA 02543
dralston@whoi.edu
phone: 508-289-2587
fax: 508-457-2194

Abstract

Field observations of flow and sediment transport in a tributary channel through intertidal mudflats indicate that suspended sediment was closely linked to advection and dispersion of a tidal salinity front. During calm weather when tidal forcing was dominant, high concentrations of suspended sediment advected up the mudflat channel in the narrow region between salty water from San Francisco Bay and much fresher runoff from the small local watershed. Salinity and suspended sediment dispersed at similar rates through each tidal inundation, such that during receding ebbs the sediment pulse had spread spatially and maximum concentrations had decreased. Net sediment transport was moderately onshore during the calm weather, as asymmetries in stratification due to tidal straining of the salinity front enhanced deposition, particularly during weaker neap tidal forcing. Sediment transport by tidal forcing was periodically altered by winter storms. During storms, strong winds from the south generated wind waves and temporarily increased suspended sediment concentrations. Increased discharge down the tributary channels due to precipitation had more lasting impact on sediment transport, supplying both buoyancy and fine sediment to the system. Net sediment transport depended on the balance between calm weather tidal forcing and perturbations by episodic storms. Net transport in the tributary channel was generally off-shore during storms and during calm weather spring tides, and on-shore during calm weather neap tides.

Keywords: sediment transport, intertidal sedimentation, salinity gradients, tidal inlets, topographic effects; San Francisco Bay, California, USA

1. Intertidal sediment transport

Sediment transport is closely linked to both the morphology and ecology of mudflats and marshes. The balance between erosion and deposition controls local bed elevation, and bed elevation with respect to mean sea level feeds back into sedimentation through inundation frequency and duration [Friedrichs and Perry, 2001]. Sediment transport mechanisms are spatially heterogeneous across the intertidal zone, from vegetated marsh surface to unvegetated mudflats to deeper subtidal channels. However, sediment fluxes among mudflat, marsh, and channel regions are coupled and depend on the hydrodynamic forcing [Yang et al., 2003]. Although field studies have documented sediment transport processes on mudflats [Christie et al., 1999; Dyer et al., 2000; Le Hir et al., 2000], and in marshes [Leonard et al., 1995a; Leonard et al., 1995b; Christiansen et al., 2000], observations remain limited because of logistical challenges with soft substrate, small and variable water depth, intermittent erosion events, and spatial variability between channels and shoals [Dyer et al., 2000].

Sedimentation in the intertidal zone depends in large part on settling and scour lag asymmetries [Postma, 1961]. Sediment advected into the intertidal zone during flood tides can settle and deposit around high water slack. Bed sediments partially consolidate during slack water such that equivalent ebb velocities may not be sufficient to resuspend deposited sediment. On marsh surfaces, vegetation reduces flow velocity and suppresses turbulence, enhancing settling and suppressing scour [Leonard and Luther, 1995]. Deposition is enhanced by flood dominant tidal velocities, when faster flood velocities of shorter duration are balanced by longer, slower ebbs. Flood dominant velocities and

settling around high water contribute to suspended sediment concentration maxima during flood tides for a range of shallow tidal systems: shallow estuaries [Chant and Stoner, 1998; Fettweis et al., 1998], mudflats [Le Hir et al., 2000; Christie et al., 1999], and marshes [Lawrence et al., 2004]. On ebb dominant mudflats, the settling and scour lag effect can generate greater sediment concentrations during floods than ebbs [Dyer et al., 2000].

Astronomical tides are not the only source of energy for intertidal sediment transport. Wind waves can generate bed stresses much greater than tidal currents alone, but the effects depend greatly on wind direction and water depth [Le Hir et al., 2000]. Because near-bed wave orbital velocities are greater in shallower depths, mudflat shoals are more exposed to wave stresses than deeper channels. Wave bed stresses suspend sediment, and tidal flows advect the increased sediment concentrations. Consequently, the timing of winds with respect to ebb/flood and spring/neap cycles impacts net transport [Leonard et al, 1995b; Le Hir et al., 2000; Yang et al., 2003]. Generally, storms (especially around high water) reverse calm weather onshore transport of sediment and drive net export of sediment from mudflats [Wells and Park, 1992; Shi and Chen, 1996; Christie et al., 1999; Dyer et al., 2000; Le Hir et al., 2000; Janssen-Stelder, 2000; Yang et al., 2003]. While erosive response to storms occurs over time scales of days, recovery to pre-storm elevations can take weeks to months [Yang et al., 2003].

Sediment transport on intertidal mudflats can be broadly summarized as varying between calm, depositional periods when tidal forcing dominates, and stormy, erosional

periods when wind waves are significant. During stormy periods, export depends both on wave stresses that suspend bed material and on water column mixing that inhibits settling around high water. However, sediment transport in mudflat channels may be significantly different than on adjacent shoals, as channels have stronger tidal velocities and are less impacted by waves. As a result, sediment exchanges between shoals and channel – mud can be stored in channels after storms [Yang et al., 2003] and during neap tides [Christie et al., 1999], and resuspended during calm and spring periods. Contrary to the intertidal zone as a whole, channels may offer conduits for export of sediment during calm conditions [Wells et al., 1990; Dyer et al., 2000].

In estuaries, the salinity distribution impact sediment transport through baroclinic circulation convergence [e.g., Schubel, 1968] or through tidal asymmetries in velocity [Jay and Musiak, 1994] and turbulent mixing [Geyer, 1993]. Sediment deposits and suspended sediment maxima are typically found near the limit of the salinity intrusion, either at low salinity [Geyer 1993; Burchard and Baumert, 1998; Chant and Stoner, 2001; Sanford et al., 2001] or in the fresh region immediately upstream of the salt field [Uncles and Stephens, 1993]. In some estuaries, maximum sediment concentrations have been found toward the middle of the salinity distribution due to lateral exchange with supplies of erodible bed sediment [Geyer et al., 1998; Blake et al., 2001]. As we present in these observations, the salinity field is closely linked to the suspended sediment distribution in a shallow mudflat channel, with peak sediment concentrations consistently in the middle of the salinity gradient, albeit over a much narrower spatial region than in most estuaries. Observations of a shallow channel in the Tavy Estuary (U.K.) also found maximum

turbidity corresponded with the middle of a relatively compact salinity field [Uncles and Stephens, 2000]. Although the Tavy channel was deeper, sediment and salinity patterns there were in many ways similar to these observations — the water column was well-mixed and highly turbid early during flood tides, and strongly stratified with decreased near-bed SSC during ebbs.

There has been relatively little research on sediment transport in channels through intertidal regions [Wells and Park, 1992, Shi and Chen, 1996; Lawrence et al., 2004]. This work documents sediment transport in a tributary mudflat channel in Central San Francisco Bay during the winter wet season, detailing both calm and stormy periods. Because of longitudinal salinity gradients generated by seasonal precipitation, the dominant hydrodynamic feature in the channel is a tidal salinity front [Ralston and Stacey, 2005a]. In this paper, we quantify dominant factors controlling sediment transport in tributary channels through the intertidal zone. We consider how hydrodynamic and estuarine processes at the tidal salinity front impact suspended sediment concentrations in mudflat channels. In addition, we compare calm weather conditions with intermittent meteorological events with increased wind and precipitation, considering how this balance between dominant tidal and meteorological forcing periods modulates net sediment flux in the mudflat channel.

2. Site Description

The observations presented here were collected during field experiments in a mudflat and salt marsh region at the University of California's Richmond Field Station

(RFS) in Central San Francisco Bay (Figure 1). In the experiments, we deployed near-bed instruments to measure velocity and scalar concentrations on the mudflats and in the subtidal channels passing through mudflat and marsh. The channels flow out of small, mostly urban watersheds, and we focus on the western channel, Meeker Slough, which has an above-ground length of 2.2 km and drains roughly 8 km^2. Tidal range at the site is about 2 m, so most of the region shown in the figure is exposed at lower low water. Water continues to flow down the channels after the tide has receded off the mudflats, with discharge in Meeker Slough estimated between 0.05 and 0.4 m^3/s during the study.

The dominant seasonal variability in the region is Mediterranean, with dry summers and wet winters. The discussion here focuses on conditions during the wet winter months when precipitation runoff enters the marsh from upstream tributary channels. During the winter, storm systems pass through the Bay Area with a periodicity of 5 to 10 days and bring precipitation and strong winds from the south or southeast [Conomos et al., 1985]. Precipitation between December and March accounts for roughly 70 percent of the annual total in the Bay Area, and helps to create a gradient in salinity between relatively fresh water draining down the tributary channels and much saltier water in San Francisco Bay. The salinity transition occurs over a narrow region, creating a strong longitudinal density gradient that persists throughout the winter months. Because of its location and open exposure Central San Francisco Bay, wave conditions at the field site are particularly sensitive to winds from the south that are commonly associated with winter storms.

3. Methods

In particular, we focus on data collected from December 19, 2003 to January 3, 2004, when instruments were deployed instrument at two locations along the channel, downstream where the channel passed through mudflats (Frame A), and upstream in the vegetated marsh (Frame B) (Figure 1). Channel depth was roughly constant through the study reach; the bed elevation at Frame A was about 0.3 m above MLLW, and at Frame B was 0.1 m above MLLW. On each frame, acoustic Doppler velocimeters (ADVs), conductivity-temperature-depth sensors (CTDs), and optical backscatter sensors (OBSs) were mounted at several elevations near the bed. On Frame A (mudflat channel) the three ADV sample volumes were located 0.10 m, 0.25 m, and 0.40 m above the bed, and the ADVs sampled at 16 Hz for 5 minute bursts every 15 minutes (0.25 m) or 30 minutes (0.10 m and 0.40 m). CTDs were fixed 0.10 m, 0.35 m, and 0.70 m above the bed, with the two lower instruments sampling every 30 seconds and the upper CTD sampling every 15 minutes. OBSs were mounted 0.10 and 0.35 m above the bed, sampling every 30 seconds and 15 minutes respectively; in post-processing, data from the lower OBS were despiked and filtered with a 2 ½ minute moving average.

On Frame B (marsh channel), two ADVs were 0.25 m and 0.40 m above the bed, sampling at 16 Hz for 5 minute bursts every 30 minutes. Frame B had CTDs 0.10 m and 0.70 m above the bed; the lower CTD sampled every 7.5 min and the upper CTD every 15 min. OBSs were mounted 0.10 m, 0.20 m, and 0.40 m above the bed and sampled every 7.5 minutes; a fourth OBS was set 0.70 m above the bed and sampled every 15 minutes. All of the instruments collected data for two weeks, but 10 days into the

experiment (December 29) a large precipitation event significantly increased flow in the channel and dislodged the frames. We limit our analyses to time before the storm.

Optical backscatter measurements are sensitive to particle size [Bunt et al., 2002], so the OBSs were calibrated using suspended sediment from the field site. Bed sediments on the mudflats ranged from clay and silt to very fine sand, but suspended material was dominated by the finer fraction [Ralston, 2005]. Laboratory and field calibrations with suspended sediment were used to convert measured OBS voltages to the reported suspended sediment concentrations (SSC). On Frame A, the lower OBS reached full scale at a sediment concentration of 1240 mg/L, while full scale for the upper OBS was 200 mg/L. Calibrations for the instruments on Frame B relied on previous work using sediment from Northern San Francisco Bay rather than samples from RFS, so conversion to suspended sediment concentrations is less robust. For this reason, and because the channel geometry is simpler at the downstream frame, we focus these analyses on data from Frame A.

Meteorological data during the experiment were collected from nearby stations. The hourly precipitation record combines data from three local stations operated by the California Department of Water Resources. Wind and air temperature were recorded at a meteorological station at RFS operated by the Bay Area Air Quality Management District. Finally, tidal stage data came from the NOAA station at Richmond (#9414863). The map of the intertidal and nearby subtidal bathymetry (Figure 1) was generated based on depth measurements during of surveys of the study area with a boat-mounted acoustic

Doppler current profiler (ADCP). Measured depths were converted to bed elevations by referencing to tidal stage at the NOAA station. Elevations are relative to NAVD 88, but they are effectively equivalent to elevation above MLLW, since it is 0.002 m below the NAVD 88 datum. Unshaded regions in the map are salt marsh that was inaccessible to ADCP transecting.

4. Results

During the study, tidal forcing was mixed semi-diurnal with amplitude of about 2 m (Figure 2a). Because of the asymmetric tides, the mudflats were exposed diurnally each lower low water (LLW); water covered much of the intertidal region at higher low waters (HLW). This distinction is important when describing conditions on the mudflats, so in the following discussion the diurnal tides are subdivided into four periods: an initial strong flood from LLW to LHW, a weak ebb toward HLW, a weak flood toward HHW, and a strong flood toward LLW at the end of the inundation.

Suspended sediment concentrations during the experiment varied from background levels of about 25 mg/L to over 1000 mg/L during storms (Figure 2). More typically, the diurnal tidal cycle variability in SSC yielded peaks of about 300 mg/L. Sediment concentrations depended on the hydrodynamic forcing and the available sediment supply, so several small wind and precipitation events during the deployment impacted salinity and suspended sediment in the channel. During calm weather, tidal inundation of the mudflats and marsh drove the dominant diurnal pattern in SSC, but intermittent increases in sediment concentration were due to precipitation and wind.

Salinity and buoyancy dynamics during the December 2003 experiment were typical of winter wet season conditions. Salinity varied tidally between about 28 psu and nearly fresh (Figure 3a). The longitudinal salinity gradient ($\partial S/\partial x$) was greatest near the tidal salinity front at the beginning of each inundation, from 20 to 40 psu/km (Figure 3b). The tidal signal for $\partial S/\partial x$ corresponded with the buoyancy frequency: $N^2 = -(g/\rho_0)(\Delta\rho/\Delta z)$, where $\Delta\rho$ is the density difference between instruments 0.10 m and 0.35 m above the bed (Figure 3c). Stratification depended on $\partial S/\partial x$ through tidal straining; advection of the salinity gradient increased N^2 during ebbs, and straining destabilized the water column and reduced N^2 during floods.

The diurnal inundation period of the intertidal zone helped create and preserve a very strong along-channel density gradient through the wet season. Although dispersion reduced the salinity gradient through each tide, a sharp front was regenerated at the beginning of each strong flood. Stratification due to tidal straining significantly damped turbulent mixing during ebbs, creating tidal asymmetries in shear, Reynolds stress, and eddy viscosity. A more complete discussion of the hydrodynamics can be found elsewhere [Ralston and Stacey, 2005a; 2005b], but the basic framework is important for considering sediment transport mechanisms.

4.1 Tidal cycle sediment transport

Suspended sediment concentrations in the mudflat channel depended both on regular tidal forcing and on intermittent perturbations driven by meteorological events.

During calm weather when meteorological forcing was absent or weak, tidal sediment transport was periodic with each inundation and was tied to advection of the salinity front. We focus on the longest continuous period during the deployment with calm winds and no rain, roughly four days of data following moderate precipitation on day 358 (Figure 4). For orientation within the tidal cycle, water surface elevation, salinity, and velocity are plotted along with suspended sediment.

During each inundation, the salinity front advanced up the channel during the strong flood and brought a spike in SSC along with the increase in salinity (e.g., t ~ 358.9). Sediment concentrations dropped to much lower levels after the front passed the instrument frame. Sediment concentrations remained low until midway through weak ebbs when SSC steadily increased and salinity steadily decreased (e.g., t ~ 359.25). Local maxima in SSC occurred around HLW, and SSC decreased when the salinity front advected back upstream during weak floods. Finally during strong ebbs, SSC rose as the salinity front passed the instruments, with maxima in the middle of the gradient (e.g., 359.7). Sediment concentrations decreased as the marsh continued to drain around LLW until the following strong flood elevated sediment concentrations. Maximum velocities during strong floods and strong ebbs were similar, about 0.4 cm/s. However, suspended sediment concentrations did not directly depend on local velocities, since peak sediment concentrations typically preceded peak flood velocities, and concentrations during inundating floods were much greater than during receding ebbs despite similar velocity magnitudes. Similarly, diurnal maxima in suspended sediment were not strictly tied to

tidal stage, but rather were most closely depended on advection of the salinity field up the channel.

4.1.1 Advection and dispersion at the salinity front

Around LLW, the salinity gradient between fresher water upstream of the marsh and saltier water downstream in the bay occurred over a very narrow region (~ 200 m), creating large $\partial S/\partial x$. In this transition zone, sediment concentrations were greatly elevated over the background concentrations, roughly 10 times the background SSC of 25 to 30 mg/L. To consider the spatial distributions of salinity and suspended sediment, we convert salinity and sediment time series to functions of distance along the channel axis by integrating velocity in time: $x = \int_0^t u(t)dt$. To do so, we assume that flow is dominantly along the channel axis, and that the time scale for longitudinal advection is short compared with the time scale for vertical mixing [Ralston and Stacey, 2005b]. The spatial distributions of salt and sediment are plotted relative to the center of each salinity front, defined here as the location of the 15 psu isohaline (Figure 5).

Three days of strong floods and strong ebbs during the calm weather period have very similar structures. As tidal stage rises from LLW, the transition zone between fresh and salty water advects up the channel and across the mudflats, passing the instruments with a narrow spike in sediment concentration. When the transition region again advects past the instruments during the strong ebb, maximum sediment concentrations are much lower than during the strong flood. During both inundating and receding tides, the sediment distribution is approximately Gaussian and is centered at the salinity front. The

link between suspended sediment and the salinity field can be seen more clearly by plotting of sediment concentration against salinity (Figure 5c). Sediment concentrations were greatest in the middle of the salinity front, between 15 and 20 psu. Similarly, during intervening weak ebbs and floods (not shown), sediment concentrations increased as the salinity front region advected toward the instrument frames. The entire frontal region did not pass the instruments during the weak ebbs and weak floods, so maximum sediment concentrations occurred near HLW slack.

The spatial spread of the transition zone between salty and fresh water through each inundation was the result of tidal dispersion that decreased the salinity gradient and suspended sediment concentrations in the front. Dispersion of the salinity gradient was due spatial correlations in salinity and velocity, both vertically because of periodic stratification and laterally due to differential advection between the channel and shoals [Ralston and Stacey, 2005a]. An analytical model assuming along-channel advection and dispersion of a salinity step function between bay and marsh water represents the spread of the front: $S(x,t) = \frac{S_0}{2}\left(1 + erf\left(\frac{x - x_c}{\sqrt{4K_x t}}\right)\right)$, where S_0 is the initial magnitude of the step and x_c advects with the center of the front. The salinity data were fit with an along channel dispersivity (K_x) of 5 to 10 m^2/s.

Similarly, evolution of the along-channel suspended sediment distribution with time can be idealized by advection and dispersion of an initial sediment spike:

$C(x,t) = \frac{M_0}{\sqrt{4K_x t}} \exp\left(-\frac{(x - x_c)^2}{4K_x t} \right)$, where M_0 is the initial mass, and x_c advects with the center of the front. The spread of the spatial distribution as measured by the variance (σ^2) provides an estimate of the along-channel dispersivity: $K_x = \frac{\sigma_2^2 - \sigma_1^2}{2(t_2 - t_1)}$ [Fischer et al., 1979]. We measure the spread of the suspended sediment peak by calculating the second moment of the along-channel concentration distribution. Because the instrument frames were relatively close to the low tide elevation, passage of the salinity front and sediment spike around low water was quickly followed by the returning flood tide. To completely capture the return to background suspended sediment concentrations away from the salinity front, we measure the width of the sediment spike on the salty side of the front. Using the change in variance during the inundation period between strong flood and strong ebb, the longitudinal dispersivity for suspended sediment was calculated to be 5 to 8 m^2/s. This estimate is consistent with the longitudinal dispersivity of salt based on the spread of the salinity gradient.

Thus, suspended sediment variability in the mudflat channel during calm weather was predominately due to advection and dispersion of a pulse of sediment centered at the tidal salinity front. Net erosion and deposition in the intertidal zone appear to be small contributions to the suspended sediment budget at tidal timescales compared with advection and tidal dispersion. We consider integration of these tidal processes over longer periods in section 5.

4.1.2 Secondary sediment maxima during floods

In both the time series and the spatial distributions, the primary spike in suspended sediment during the strong flood was followed by a second, but distinct, local maximum. The secondary peak followed approximately 50 minutes after the maximum sediment concentration (Figure 4c); this corresponded with a spatial lag of 500 to 700 m (Figure 5b). The secondary maxima occurred behind the salinity front every day, and we focus on one such sequence during a strong flood (Figure 6). In this case, the secondary peak (t ~ 361.025) was roughly half the sediment concentration in the salinity front (t ~ 360.99). The secondary maximum was distinct from the salinity front, and between the two peaks, bay water advected past the instruments with relatively constant near-bed salinity and velocity. However, near-bed water temperature during this period mirrored the variability in suspended sediment (Figure 6b). Temperature decreased rapidly when sediment concentrations increased, and slowly rose as sediment concentrations decreased.

During the field deployment, inundation of the mudflats began each night when air temperature was significantly lower than the water temperature (Figure 6b). As a result, near-surface water in contact with the night air cooled more rapidly than near-bed water. Periods of strong vertical mixing redistributed cool near-surface water downward as well as suspended sediment. Mixing at the salinity front produced the initial increase in suspended sediment and decrease in near-bed temperature. However, immediately behind the salinity front, the water column was salinity stratified and turbulent mixing was suppressed (Figure 6c). Only when stratification decreased did vertical mixing increase, yielding both increased suspended sediment and decreased near-bed temperature.

Salinity stratification behind the flood front was a regular feature during the wet season. Differential advection of the salinity front between channel and shoals created lateral density gradients and forced lateral baroclinic circulation, with flow out of the channel near the bed and convergent at the surface [Ralston and Stacey, 2005a]. The lateral exchange enhanced stratification behind the front, and helped create the secondary peak in suspended sediment. When the water column was stratified behind the front, near-bed flow was relatively warm with low suspended sediment concentrations. When the water column mixed vertically, near-surface water that was cooler and had higher sediment concentrations mixed downward toward the sensors.

The instruments were positioned in the center of the channel, so we cannot directly address the source of the sediment in the secondary maximum. The secondary peak typically occurred when water depth in the channel was about 0.7 m, and at this depth the shoals adjacent to the instrument frames were shallowly inundated. Because of the close proximity to the salt marsh, the channel banks near the instrument frame were narrower and deeper than farther downstream on the mudflats. At the time of the secondary peak, shallow flow on the shoals provided a source of cool, sediment-laden water for advection into the channel, and mixing at the relatively steep channel banks could have contributed to the breakdown of stratification behind the front. Without measurements across the bathymetric gradient, though, we cannot determine the channel-shoal exchange. Sediment concentrations in the secondary maxima were much lower

than in the salinity front, and tidal dispersion smoothed the gradient between the two peaks by the time the tide receded during strong ebbs.

4.2 Episodic forcing

Description of the tidal cycle sediment transport in the previous section focused on a period of relatively calm weather, with light winds and little precipitation. Winter storms perturb the tidal cycle pattern by altering both the hydrodynamics and the sediment supply in the intertidal zone. Winter storms greatly increased suspended sediment on the mudflats – the highest sediment concentrations during the observations were during and immediately after storms (Figure 2). Storms added sediment to the water column both by eroding bed material by wind waves and by delivering sediment with precipitation runoff down the tributary channels. Increased freshwater discharge due to runoff after storms also strengthened $\partial S/\partial x$ (Figure 3), impacting the buoyancy dynamics in the channel. The response of the system to these episodic events can be considered in the context of the tidal cycle pattern, with changes in buoyancy and sediment supply as perturbations to the calm weather exchange.

4.3.1 Wind: sediment suspension

In shallow water, wind waves can create significant bed stresses that erode sediment and mix the water column vertically. Wind waves suspend sediment both on the mudflats and in the shallow subtidal region offshore, increasing sediment concentrations advected across the intertidal zone during floods. Winter storms bring winds from the south, but prevailing winds are generally from the north. The mudflats at

the field site face south, and are sheltered by land, marsh, or breakwaters on the other three sides. Consequently, sediment transport response to wind depended greatly on wind direction. Winds from the north and east had very limited fetch to generate wind waves. The channel orientation was approximately east-west as it entered the mudflats, so flow there was moderately sensitive to wind along this axis. For example, wind from the east pushed water up the channel around low water, increasing the depth, salinity, and suspended sediment at the instruments (Figure 2, brief increase in water depth at t ~ 354.6).

Only winds from the south significantly altered suspended sediment patterns in the channel. We focus on conditions in the channel during one storm period (Figure 7). Although strong winds from the south began around HHW, sediment concentrations advecting past the instruments during the ebb were relatively unaffected because flow in the marsh remained sheltered by breakwaters and vegetation. However, wind waves suspended sediment offshore in the shallow subtidal region, and during the following flood, maximum sediment concentrations at the front were more than twice the concentrations typical of calm weather. The elevated sediment concentrations preceded the precipitation, so the likely source was bed erosion by wind waves rather than terrestrial runoff or direct impact of raindrops on exposed mudflat. Suspended sediment concentrations in the channel remained elevated throughout the strong southerly wind, but local maxima still coincided with the salinity gradient. Shortly after the winds dropped, sediment concentrations decreased to levels more typical of the tidal forcing.

4.3.2 Precipitation: buoyancy and sediment supply

In addition to wind, winter storms brought precipitation. Runoff increased freshwater discharge in the tributary mudflat channels, and supplied both buoyancy and terrestrial sediment to the intertidal region. For example, moderate precipitation on day 358 altered both salinity and sediment conditions in the channel (Figure 8). Early in the strong ebb, suspended sediment concentrations were low and the water column was salinity stratified (t ~ 358.58). However with the storm, precipitation and wind from the south intensified, and near-bed sediment concentrations increased rapidly (t ~ 358.595, #1). Fresh, sediment-laden runoff mixed vertically downward from the surface, increasing near-bed sediment concentrations and decreasing near-bed salinity. The near-surface layer had been warmed by the afternoon air, so when it mixed downward, near-bed temperature increased. Mixing of sediment, salinity, and temperature over the water column was due to wind waves shoaling and breaking on the shallow mudflats.

After a brief period when sediment concentrations were high and the water column was vertically mixed, near-bed suspended sediment rapidly decreased at the same time that the water column restratified (t ~ 358.605, #2). Near-bed suspended sediment decreased, salinity increased, and temperature decreased, all corresponding with flow reversal near the bed as the lowest ADV returned to flooding velocities while the surface layer continued to ebb. The flow reversal was driven by dense bay water advected up onto the mudflats by the wind from the south, as the wind-setup in combination with increased freshwater discharge significantly strengthened the baroclinic pressure gradient in the channel. As bay water advected upstream toward the marsh, near-bed sediment

concentrations decreased and the fresher, sediment-laden runoff was again confined to a surface layer. Sediment concentration near the bed remained relatively low until much later in the ebb, when the entire water column was again ebbing and the channel mixed vertically due to falling water level and increasing velocity (t ~ 358.64, #3). Upstream in the marsh at frame B conditions were similar during this period – the water column restratified midway through the ebb and near-bed flow reversed, and near-bed sediment concentration decreased simultaneously. During the storm, the combination of increased discharge, wind-driven setup, and wind wave mixing altered the hydrodynamics, while terrestrial runoff increased the available supply of suspended sediment in the channel.

5. Analysis of sediment fluxes

Because of particle settling, suspended sediment is not necessarily conserved in the water column. Suspended sediment at the field site consisted predominantly of clays and fine silt, with dominant particle diameters around 10 μm [Ralston, 2005]. Fine cohesive sediments like these tend to aggregate into large, low density flocs that settle faster than individual particles. Flocs on the order of 100 μm diameter are common in San Francisco Bay, but sizes can range from 10 to 1000 μm [Kranck and Milligan, 1992; Gartner et al., 2001]. Field estimates of floc settling rates found velocities of 0.1 to 0.5 mm/s for floc diameters of about 150 μm in the coastal ocean off Northern California [Sternberg et al., 1999; Hill et al., 2000].

Assuming settling velocities of 0.1 to 0.5 mm/s and a water depth of 2 m, the time scale for settling to remove all suspended sediment from the water column is between 1

and 5 hours, significantly less than the daily inundation period. However, total sediment in the salinity front did not substantially change between inundating and receding tides (Figure 5b). Although dispersion spread the initial sediment spikes spatially, the integral of near-bed suspended sediment concentration remained largely unchanged between strong floods and strong ebbs. Given the shallow depth, settling during the diurnal inundation could remove most suspended sediment from a quiescent water column. However, turbulent mixing in the mudflat channel appears sufficient to keep most of the sediment at the salinity front in suspension.

The ratio of the settling velocity to the friction velocity provides a scale for the balance between mixing and particle settling. Specifically, the Rouse number is $P = {w_s}/{\kappa u_*}$, where w_s is the settling velocity, u_* is the friction velocity, and κ is von Karman's constant (0.4). If we set the friction velocity equal to the square root of the Reynolds stress at the lowest ADV ($u_* \sim \sqrt{\overline{u'w'}_{10\,cm}}$), and assume w_s ~ 0.5 mm/s, then the resulting Rouse number was much less than one for most of the experiment (Figure 9b). For Rouse numbers much less than 1, sediment is suspended throughout the water column; for Rouse numbers much greater than 1, settling dominates vertical mixing and suspended sediment is concentrated near the bed. The Rouse number has been filtered with a 3-hour moving average, assuming this is a relevant time scale for settling across the water column. The time series modulated with the spring-neap variability in tidal forcing and turbulent mixing. Rouse numbers were lowest during the middle of the deployment around day 358 when tidal amplitudes were greatest; additionally, wind and freshwater discharge increased near-bed stresses around this time. Rouse numbers

increased during the calm weather period, coinciding with lower tidal amplitudes during the neap.

Although sediment transport in the channel at diurnal timescales is dominated by tidal advection and dispersion, we can quantify small differences in transport between tidal cycles by calculating cumulative sediment flux past the instrument frame. Velocity and sediment concentrations were measured at fixed elevations in the center of the channel, so we must make several simplifying assumptions to estimate the mass flux. We assume flow is dominantly along the channel axis, uniform across the channel, and that the velocity profile is logarithmic. We also assume the vertical distribution of suspended sediment follows the Rouse profile: $C(z) = C(a)\left[\frac{h-z}{z}\frac{a}{h-a}\right]^{P/\beta}$, where concentration at elevation z is relative to the concentration at reference elevation a; h is the water depth, P is the Rouse number, and β is a coefficient assumed equal to 1. Taking the OBS at 0.10 m above the bed for the reference sediment concentration, we multiply the resulting sediment profile by the velocity profile calculated from the ADV measurements to get the sediment flux through time.

Keeping in mind the limitations of these assumptions, the resulting estimate of cumulative sediment flux shows effects of the episodic storms and of the spring-neap transition in turbulent mixing (Figure 9c). The cumulative flux is relative to the arbitrary zero of the beginning of the deployment, so periods with positive slopes indicate net on-shore transport while periods with negative slopes have net off-shore transport. The largest magnitude shifts in sediment flux are associated with precipitation, with greatly

increased export associated with storms during the middle (days 357 to 358) and at the end (day 363) of the observations. Between the storms, the direction of net transport in the channel depended on the strength of the tidal forcing. Early in the deployment, cumulative transport was generally offshore (slope < 0); this corresponded with a period of spring tides, but the effect of increased tidal amplitude may have been enhanced by wave stress due to moderate winds from the east during this period. During the calm weather period with relatively weak tidal forcing, net transport in the channel was slightly onshore (slope > 0). Onshore transport during the calm period corresponds with higher Rouse numbers, with sediment deposition more likely when Reynolds stresses decreased due to weaker neap tides and stronger periodic stratification.

6. Discussion

Based on the calm weather tidal forcing and the episodic perturbations by storms, we can begin to describe sediment transport in the mudflat channel during the wet season. Maximum sediment concentrations typically corresponded with the location of the sharp salinity gradient between fresh discharge and saltier bay water. Through each daily inundation, the region of suspended sediment and salinity gradient advected across the intertidal zone and dispersed longitudinally.

A conceptual model for sediment transport in this system incorporates both the tidal and episodic forcing regimes. With each winter storm, freshwater runoff delivers a pulse of sediment down the tributary channel to the intertidal and nearby subtidal areas. The bathymetry is such that the mudflat channel becomes progressively shallower and

eventually disappears where it intersects the subtidal zone, so flow from the channel expands radially and velocities decrease where it enters the bay. As a result, some of the suspended sediment ebbing down the channel around low water is likely to deposit immediately offshore of the mudflats. This store of sediment is then available for resuspension in the salinity front at the beginning of the following strong flood.

Deposition offshore during ebbs and suspension at the flood front are both enhanced by dynamics at the strong salinity gradient. During ebbs, tidal straining increases stable stratification, reduces turbulent mixing, and enhances sediment deposition [Geyer, 1993]. Periodic stratification is stronger and lasts longer during ebbs of neap tides, when tidal mixing and near-bed turbulence are weaker. Consequently, deposition rates are greater during neaps, consistent with the net flux calculations in the channel.

During floods, tidal straining reduces stratification. Advection of the salinity gradient can create unstable density profiles that mix near-surface water downward and enhance turbulence near the bed. The salinity sensors in the mudflat channel recorded unstable density profiles around passage of the front during strong floods (Figure 3c), and strong vertical velocities can increase sediment resuspension at salinity fronts [Largier, 1993]. Because $\partial S/\partial x$ was greatest around low water at the start of the inundating flood, the active turbulence at the front could suspended local sediment deposits or could vertically mix sediment associated with relatively fresh discharge down the channel at the end of the strong ebb.

Unfortunately, the instruments were positioned upstream in the mudflat channel and could not observe creation of the sediment spike in the flooding salinity front. Local bed erosion near the instrument frames did not significantly contribute to the sediment maxima in the front, since peak sediment concentrations preceded maximum shear stresses. Instead, the tidal sediment transport pattern may depend on expansion of channelized flow as it enters the bay and an associated supply of mobile sediment just offshore of the mudflats. During each inundation the sediment spike advects, disperses, and some small fraction may deposit in the intertidal zone depending on the tidal and wave energy. During the calm period of these observations, the tidal forcing regime appeared to be moderately depositional. Fine sediment that entered the system with precipitation runoff prior to the calm period was gradually redistributed to depositional areas on the mudflats or marsh or was exported offshore. However, most of the sediment suspended at the salinity front simply sloshed back and forth across the intertidal zone, and large shifts in net transport resulted from storm events.

The mudflat channels at the field site are tributaries of small watersheds, but many tidal channels around San Francisco Bay are created and maintained strictly by tidal flows [Atwater et al., 1979]. Salinity, and therefore sediment dynamics in channels without freshwater discharge are likely very different from conditions described here. For example, the seasonal sediment transport patterns on extensive mudflats in nearby San Pablo Bay are unlike those at the field site [Krone, 1979; Thompson-Becker and Luoma, 1985]. In San Pablo Bay, wind forcing dominates transport during summer

months, and fine sediment is supplied from the Sacramento River offshore of the mudflats rather than from local runoff. At field site, tributary channels deliver fine sediment, and southerly winds have the greatest impact during the winter. Tidal salinity fronts are important to sediment transport in mudflat channels with freshwater input, but are not necessarily present in all intertidal regions.

7. Summary

On mudflats at edge of Central San Francisco Bay, sediment transport in a shallow tributary channel was tied to advection and dispersion of a tidal salinity front, but was modulated by wind and precipitation associated with winter storms. During calm weather, the highest suspended sediment concentrations were in the frontal zone that advected up the intertidal zone and back out to the bay each inundation period. Along-channel dispersion of suspended sediment corresponded with dispersion of the longitudinal salinity gradient. Net sediment transport was slightly onshore during the calm weather, as asymmetries in stratification due to tidal straining of the salinity front, particularly during the relatively weak neap tidal forcing, enhanced deposition. Additionally, a secondary maximum in suspended sediment during floods resulted from exchange between the mudflat channel and shoals after the breakdown of stratification immediately behind the salinity front.

The regular sediment transport by tidal forcing was periodically altered by winter storms. During storms, strong winds from the south generated wind waves and temporarily increased suspended sediment concentrations. However, because of the

south-facing orientation of the field site, the more common seasonal winds from the north and northwest had negligible impact on sediment suspension and transport. Increased discharge down the tributary channels due to precipitation during storms had more lasting impact on sediment transport conditions, supplying both buoyancy and fine sediment to the system. Net sediment transport depended on the balance between calm weather tidal forcing and episodic storms, and therefore should vary with the season (freshwater input and prevailing wind direction), and the location (tributary or strictly tidal mudflat channels) and orientation (relative to prevailing winds) of a given intertidal region.

Acknowledgements

The authors thank Matt Brennan, Jon Fram, Maureen Martin, Deanna Sereno, and Stefan Talke for field assistance, and are grateful to John Trowbridge for helpful discussions. The research was funded by National Institutes of Health grant P42ES0475 from the National Institute of Environmental Health Sciences.

References

Atwater, B.F., Conard, S.G., Dowden, J.N., Hedel, C.W., MacDonald, R.L., Savage, W., 1979. History, landforms, and vegetation of the estuary's tidal marshes. In: Conomos, T.J. (Ed.), San Francisco Bay: The Urbanized Estuary. American Association for the Advancement of Science, San Francisco, pp. 347-386.

Blake, A.C., Kineke, G.C., Milligan, T.G., Alexander, C.R., 2001. Sediment trapping and transport in the ACE Basin, South Carolina. *Estuaries,* 24(5), 721-733.

Bunt, J.A.C., Larcombe, P., Jago, C.F., 1999. Quantifying the response of optical backscatter devices and transmissometers to variations in suspended particulate matter. *Continental Shelf Research*, 19, 1199-1220.

Burchard, H., Baumert, H., 1998. The formation of estuarine turbidity maxima due to density effects in the salt wedge. A hydrodynamic process study. *Journal of Physical Oceanography*, 28, 309-321.

Chant, R.J., Stoner, A.W., 2001. Particle trapping in a stratified flood-dominated estuary, *Journal of Marine Research*, 59, 29-51.

Christiansen, T., Wiberg, P.L., Milligan, T.G. 2000. Flow and sediment transport on a tidal salt marsh surface. *Estuarine Coastal and Shelf Science*, 50, 315-331.

Christie, M.C., Dyer, K.R., Turner, P., 1999. Sediment flux measurements from a macro tidal mudflat. *Estuarine Coastal Shelf Science*, 49, 667-688.

Conomos, T.J., Smith, R.E., Gartner, J.W., 1985. Environmental setting of San Francisco Bay, *Hydrobiologia*, 129, 1-12.

Dyer, K.R., Christie, M.C., Feates, N., Fennessy, M.J., Pejrup, M., van der Lee, W., 2000. An investigation into processes influencing the morphodynamics of an intertidal mudflat, the Dollard Estuary, The Netherlands: I. hydrodynamics and suspended sediment. *Estuarine Coastal and Shelf Science*, 50, 607-625.

Fettweis, M., Sas, M., Monbaliu, J., 1998. Seasonal, neap-spring and tidal variation of cohesive sediment concentration in the Scheldt Estuary, Belgium. *Estuarine, Coastal and Shelf Science*. 47(3): 21-36.

Fischer, H.B., List, E.J., Koh, R.C.Y., Imberger, J., Brooks, N.H., 1979. Mixing in Inland and Coastal Waters. Academic Press, San Diego.

Friedrichs, C.T., Perry, J.E., 2001. Tidal salt marsh morphodynamics: a synthesis. *Journal of Coastal Research*, SI 27, 7-37.

Gabet, E.J., 1998. Lateral migration and bank erosion in a salt marsh tidal channel in San Francisco Bay, California. *Estuaries*, 21(4B), 745-753.

Gartner, J.W., Cheng, R.T., Wang, P.F., Richter, K., 2001. Laboratory and field evaluations of the LISST-100 instrument for suspended particle size determinations. *Marine Geology*, 175, 199-219.

Geyer, W.R., 1993. The importance of suppression of turbulence by stratification on the estuarine turbidity maximum. *Estuaries*, 16, 113-125.

Geyer, W.R., Signell, R.P., Kineke, G.C., 1998. Lateral trapping of sediment in a partially mixed estuary. In: Dronkers, J. and Scheffers, M. (Eds.), Physics of Estuaries and Coastal Seas, Balkema, Rotterdam, pp. 115-124.

Hill P.S., Milligan, T.G., Geyer, W.R., 2000. Controls on effective settling velocity of suspended sediment in the Eel River flood plume, *Continental Shelf Research*., 20, 2095-2111.

Jay, D.A., Musiak, J.D., 1994. Particle trapping in estuarine tidal flows. *Journal Geophysical Research*, 99(C10), 20445-20461.

Janssen-Stelder, B., 2000. The effect of different hydrodynamic conditions on the morphodynamics of a tidal mudflat in the Dutch Wadden Sea. *Continental Shelf Research*., 20, 1461-1478.

Kranck, K., Milligan, T.G., 1992. Characteristics of suspended particles at an 11-hour anchor station in San Francisco Bay, California. *Journal Geophysical Research*, 97(C7), 11373-11382.

Krone, R.B., 1979. Sedimentation in the San Francisco Bay system. In: Conomos, T.J. (Ed.), San Francisco Bay: The Urbanized Estuary. American Association for the Advancement of Science, San Francisco, pp. 85-96

Largier, J.L., 1993. Estuarine fronts: how important are they? *Estuaries*, 16(1), 1-11.

Lawrence, D.S.L., Allen, J.R.L., Havelock, G.M., 2004. Salt marsh morphodynamics: an investigation of tidal flows and marsh channel equilibrium. *Journal of Coastal Research*, 20(1), 301-316.

Le Hir, P., Roberts, W., Cazaillet, O., Christie, M., Bassoullet, P., Bacher, C., 2000. Characterization of intertidal flat hydrodynamics. *Continental Shelf Research*, 20, 1433-1459.

Leonard, L.A., Luther, M.E., 1995. Flow dynamics in tidal marsh canopies. *Limnology and Oceanography*, 40(8), 1474-1484.

Leonard, L.A., Hine, A.C., Luther, M.E., 1995a. Surficial sediment transport and deposition processes in a Juncus roemerianus marsh, west-central Florida. *Journal of Coastal Research*, 11(2), 322-336.

Leonard, L.A., Hine, A.C., Luther, M.E., Stumpf, R.P., Wright, E.E., 1995b. Sediment transport processes in a west-central Florida open marine marsh tidal creek; the role of tides and extra-tropical storms. *Estuarine Coastal and Shelf Science*, 41, 225-248.

Leopold, L.B., Collins, J.N., Collins, L.M., 1993. Hydrology of some tidal channels in estuarine marshland near San Francisco. *Catena*, 20, 469-493.

Postma, H., 1961. Transport and accumulation of suspended matter in the Dutch Wadden Sea. *Netherlands Journal of Sea Res*earch, 1, 148-190.

Ralston, D.K., 2005. Hydrodynamics and scalar transport in subtidal channels through intertidal mudflats, Ph.D. thesis, University of California, Berkeley.

Ralston, D.K., Stacey, M.T., 2005a. Longitudinal dispersion and lateral circulation in the intertidal zone. *Journal of Geophysical Research*, 110, C07015, doi:10.1029/2005JC002888.

Ralston, D.K., Stacey, M.T., 2005b. Stratification and turbulence in subtidal channels through intertidal mudflats. *Journal of Geophysical Research,* 110, C08009, doi:10.1029/2004JC002650.

Sanford, L.P., Suttles, S.E., Halkma, J.P., 2001. Reconsidering the physics of the Chesapeake Bay estuarine turbidity maximum. *Estuaries*, 24(5), 655-669.

Schubel, J.R., 1968. Turbidity maximum of the northern Chesapeake Bay. *Science*, 161, 1013-1015.

Shi, Z., Chen, J.Y., 1996. Morphodynamics and sediment dynamics on intertidal mudflats in China (1961-1994). *Continental Shelf Research*, 16(15), 1909-1926.

Sternberg, R.W., Berhane, I., Ogston, A.S., 1999. Measurement of size and settling velocity of suspended aggregates on the northern California continental shelf. *Marine Geology*, 154, 43-53.

Thompson-Becker, E.A., Luoma, S.N., 1985. Temporal fluctuations in grain-size, organic materials and iron concentrations in intertidal surface sediment of San Francisco Bay. *Hydrobiologia*, 129, 91-107.

Uncles, R.J., Stephens, J.A., 1993. The freshwater-saltwater interface and its relationship to the turbidity maximum in the Tamar Estuary, United Kingdom. *Estuaries*, 16(1), 126-141.

Uncles, R.J., Stephens, J.A., 2000. Observations of currents, salinity, turbidity and intertidal mudflat characteristics and properties in the Tavy Estuary, UK. *Continental Shelf Research*, 20, 1531-1549.

Wells, J.T., Park, Y.A., 1992. Observations on shelf and subtidal channel flow: implications of sediment dispersal seaward of the Keum River Estuary, Korea. *Estuarine Coastal and Shelf Science*, 34, 365-379.

Wells, J.T., Adams, C.E., Park, Y.A., Frankenberger, E.W., 1990. Morphology, sedimentology and tidal channel processes on a high-tide-range mudflat, west coast of South Korea. *Marine Geology*, 95, 111-130.

Yang, S.-L., Friedrichs, C.T., Shi, Z., Ding, P.-X., Zhu, J., Zhao, Q.-Y. 2003. Morphological response of tidal marshes, flats, and channels of the Outer Yangtze River mouth to a major storm. *Estuaries*, 26(6), 1416-1425.

Figures

Figure 1

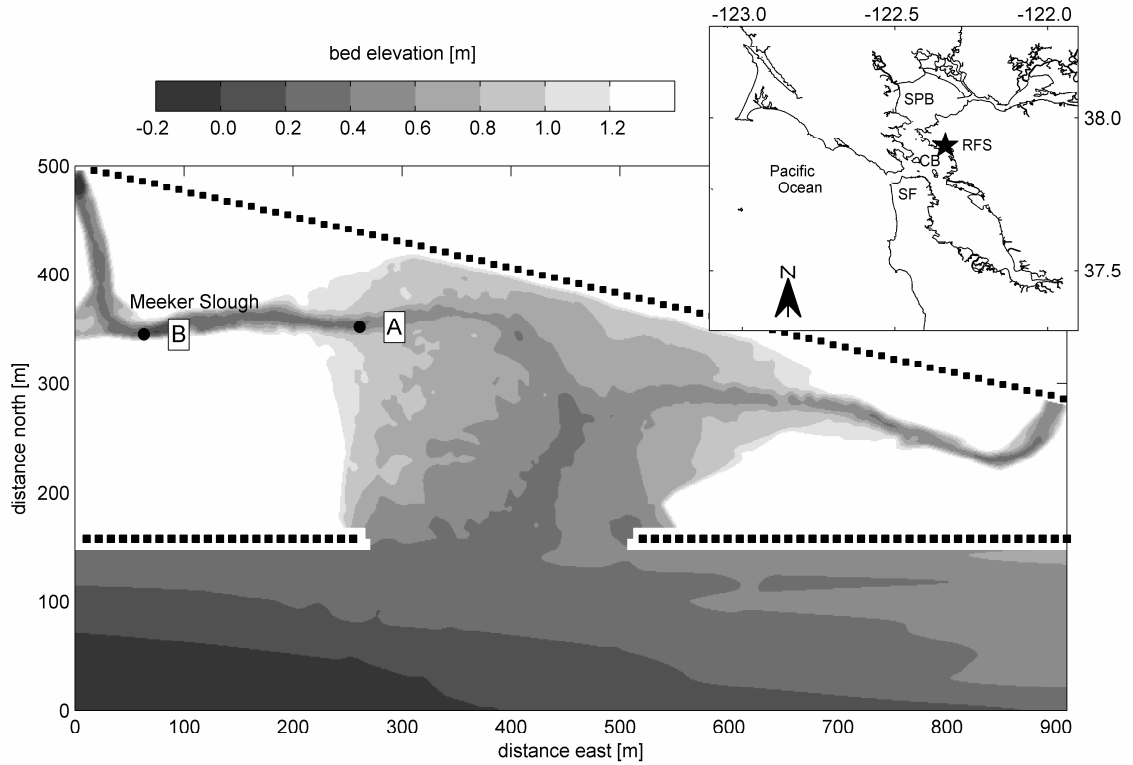

Figure 1. Intertidal mudflat bathymetry at Richmond Field Station (RFS, ★) on the eastern shore of Central San Francisco Bay (CB) and south of San Pablo Bay (SPB). Instrument frames (A and B) and breakwaters (■) are marked; salt marsh area is white.

Figure 2

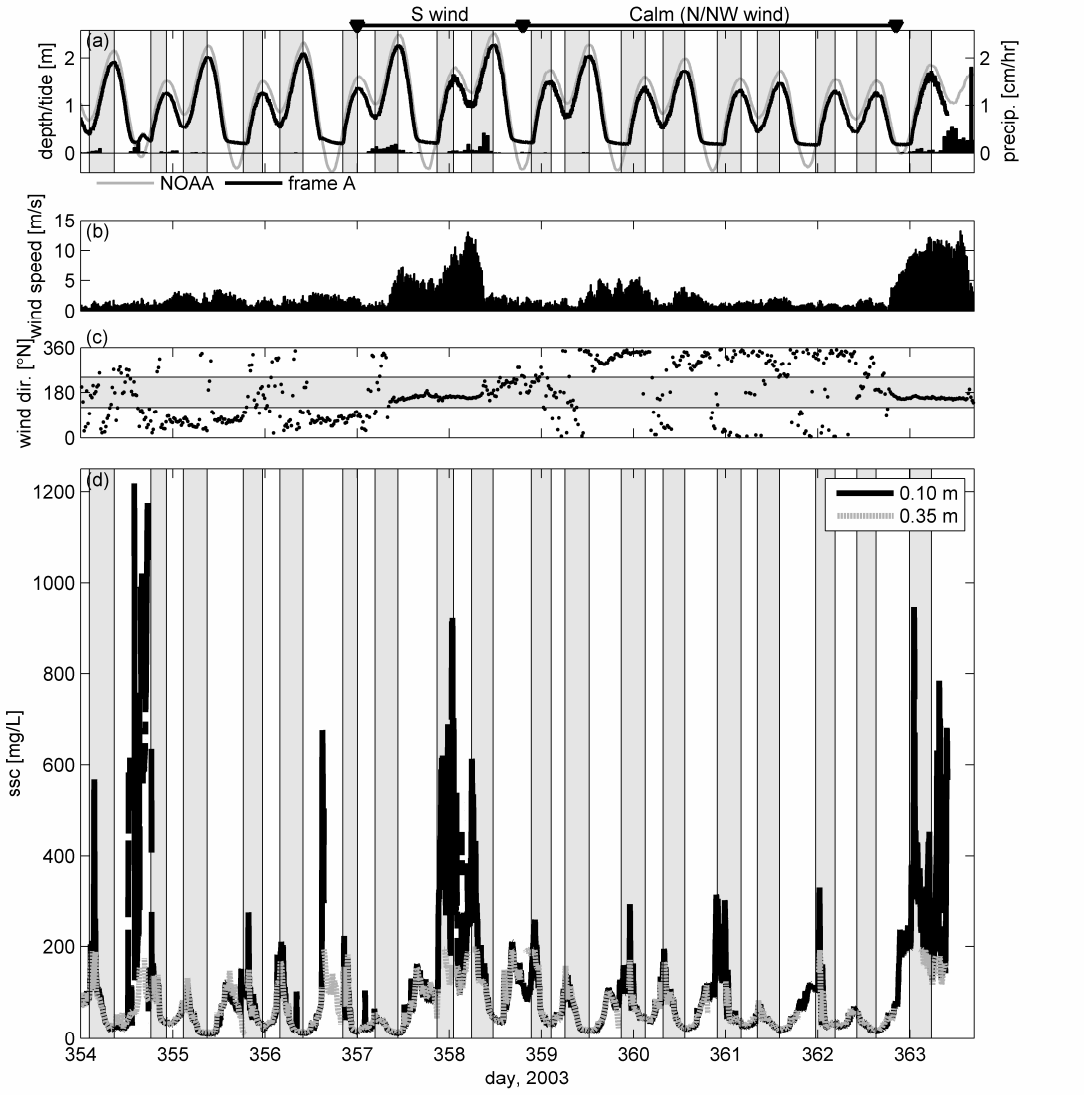

Figure 2. Suspended sediment observations in the mudflat channel. (a) Water surface in the channel, tidal stage at NOAA station, and precipitation; (b) wind speed; (c) wind direction; and (d) suspended sediment concentration 0.10 m and 0.35 m above the bed at Frame A. Forcing periods shown in greater detail are noted above (a): calm conditions (Figure 4), wind from the south (Figure 8).

Figure 3

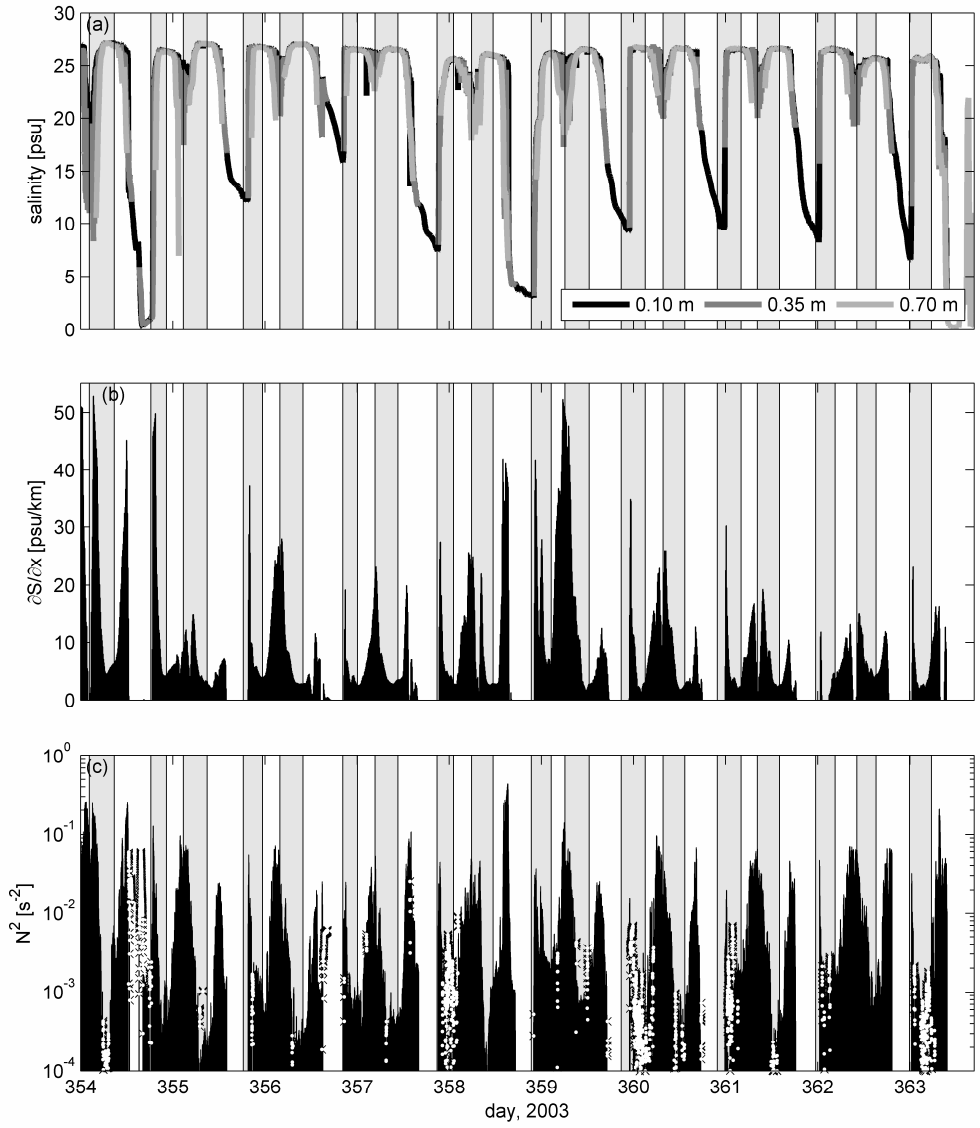

Figure 3. Salinity and stratification. (a) Salinity 0.10 m, 0.35 m, and 70 m above the bed on Frame A; (b) longitudinal salinity gradient ($\partial S/\partial x$) between frames A and B, 0.10 m above the bed; (c) stratification (N^2) between the bottom two salinity sensors on Frame A, with instances of unstable ($N^2 < 0$) marked in white.

Figure 4

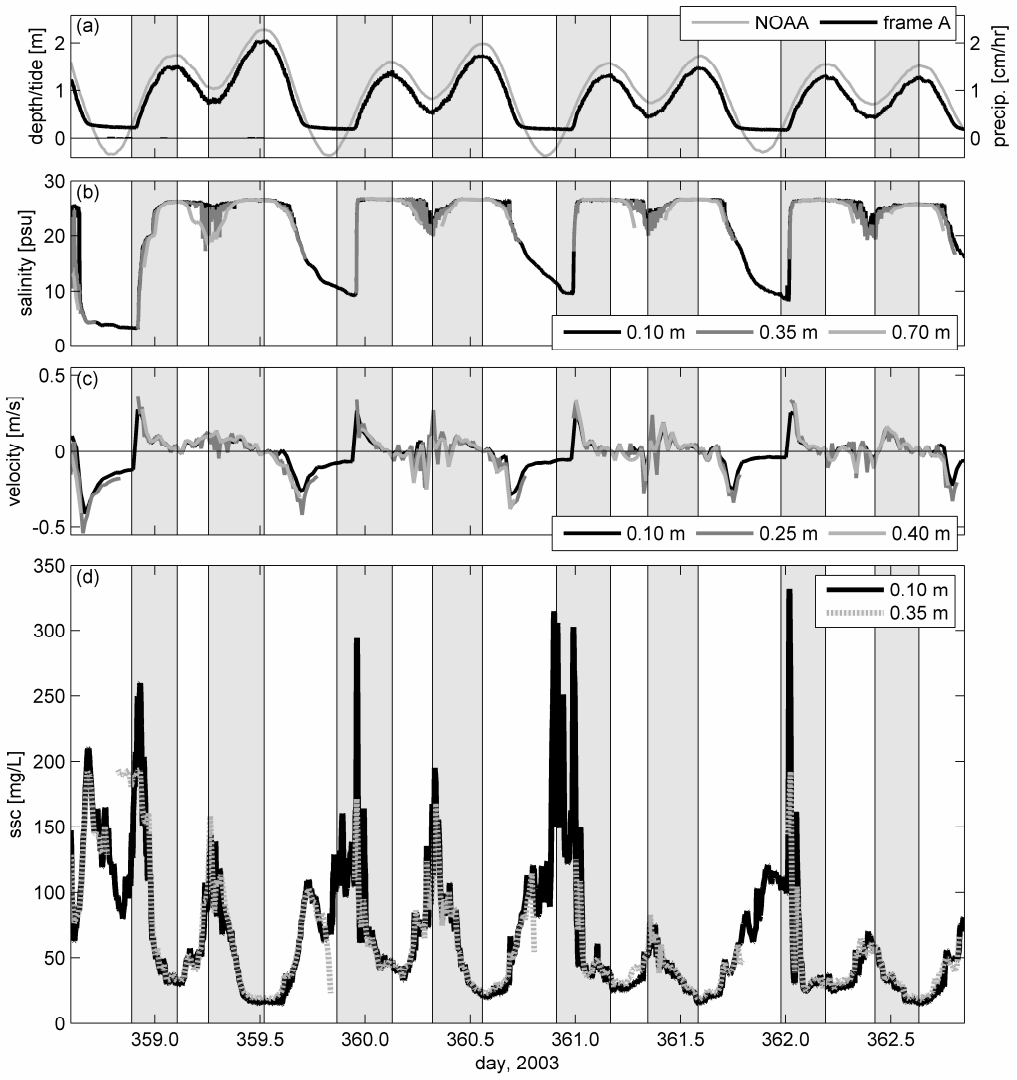

Figure 4. Conditions in mudflat channel during calm weather conditions. (a) Water surface in the channel, tidal stage, and precipitation; (b) salinity 0.10 m, 0.35 m, and 0.70 m above the bed on Frame A; (c) along-channel velocity 0.10 m, 0.25 m, and 0.40 m above the bed; (d) suspended sediment concentration 0.10 m and 0.35 m above the bed.

Figure 5

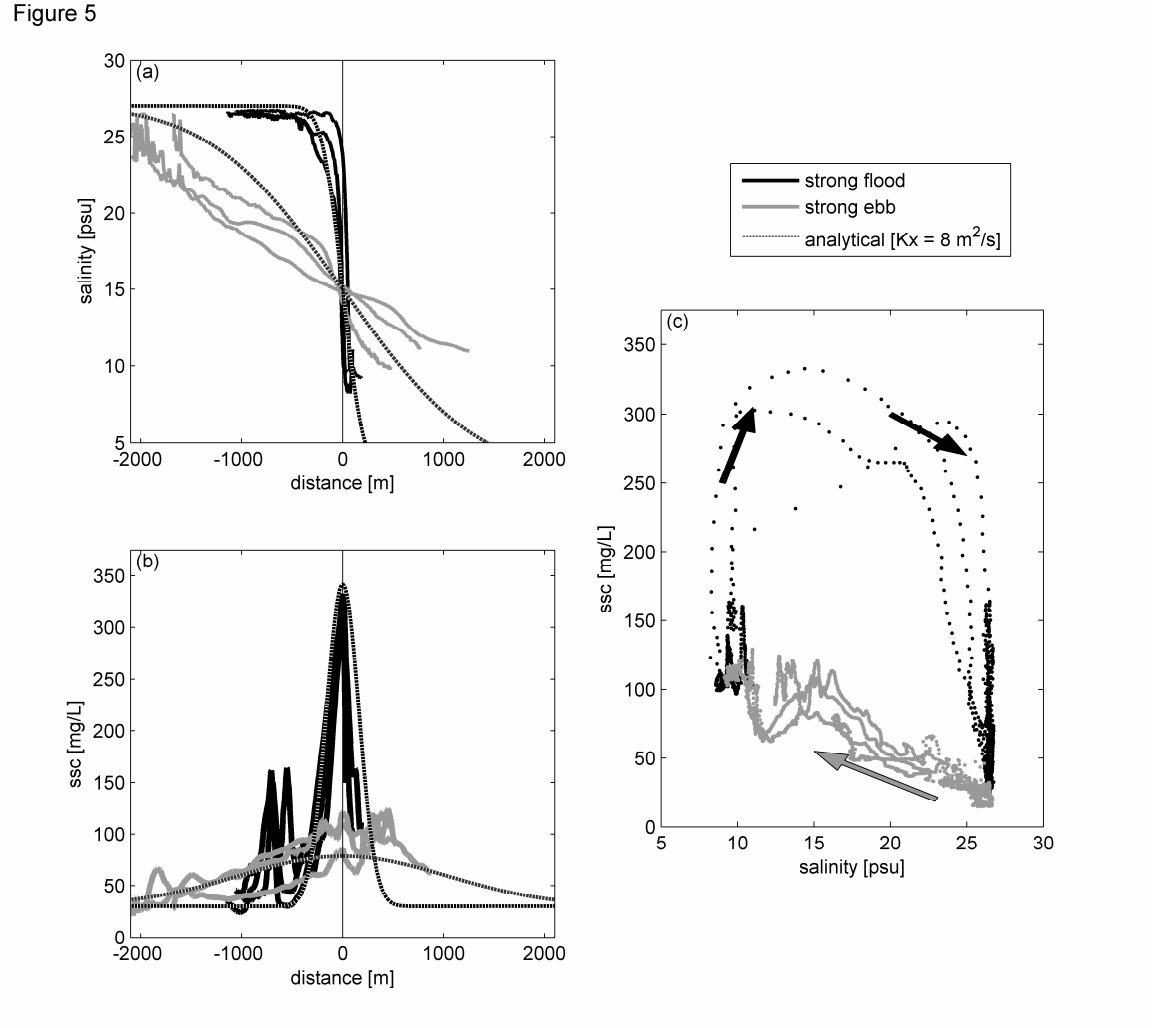

Figure 5. Salinity and suspended sediment front during calm conditions. (a) Spatial distribution of salinity during strong floods and strong ebbs; (b) spatial distribution of suspended sediment during strong floods and strong ebbs. The salinity and sediment distributions are calculated from time series at Frame A assuming advection by the local velocity; each day's observation is plotted relative to the location of the 15 psu isohaline, dashed lines represent analytical dispersion with K_x = 8 m^2/s. (c) Suspended sediment as a function of salinity; arrows indicate progression of time/distance.

Figure 6

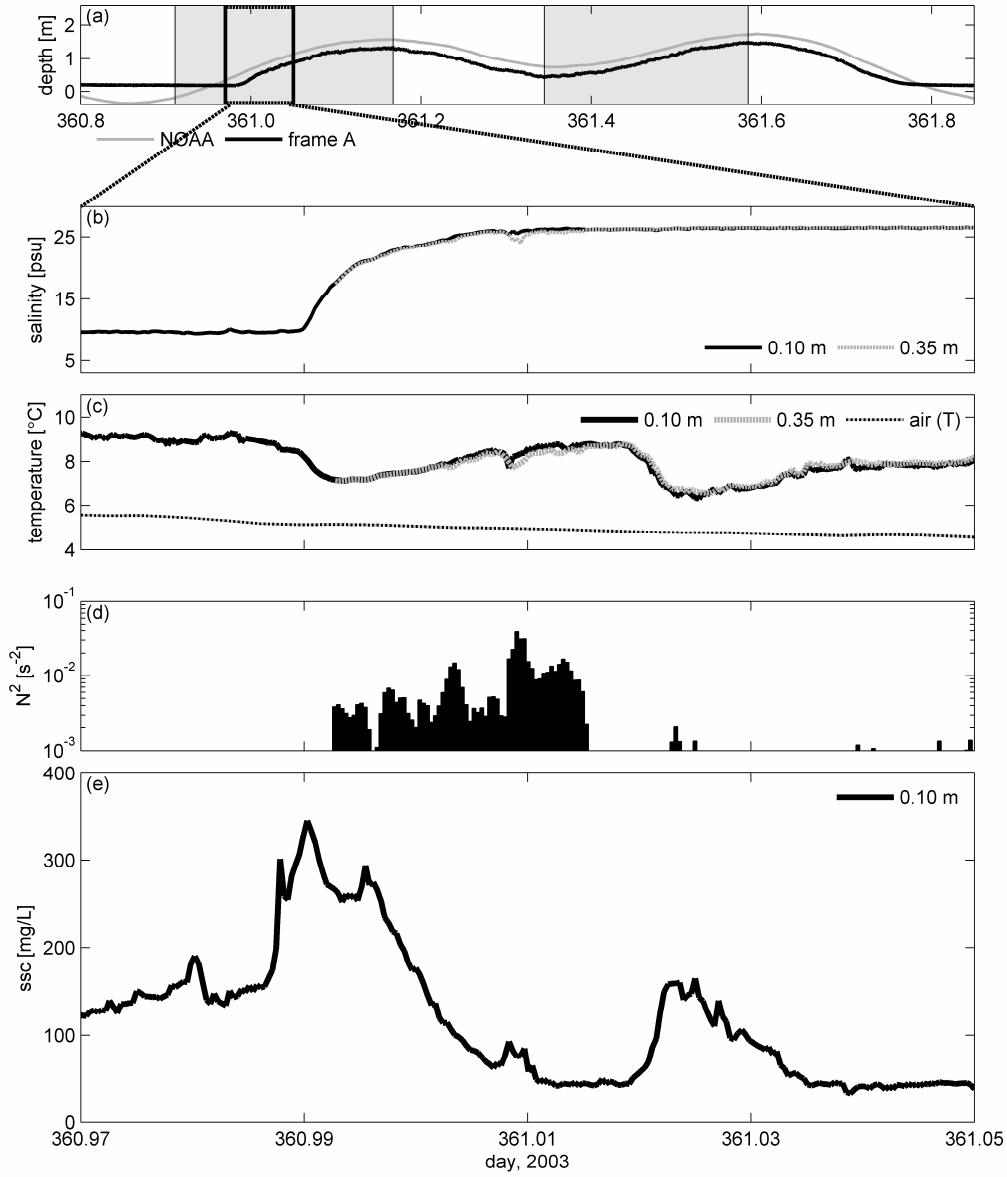

Figure 6. Detail of secondary peak in suspended sediment during strong floods. (a) Depth and tidal stage for the entire inundation, with the period in the lower panels highlighted. (b) Salinity 0.10 m and 0.35 m above the bed; (c) temperature 0.10 m and 0.35 m above the bed along with air temperature; (d) stratification; (e) suspended sediment 0.10 m above the bed.

Figure 7

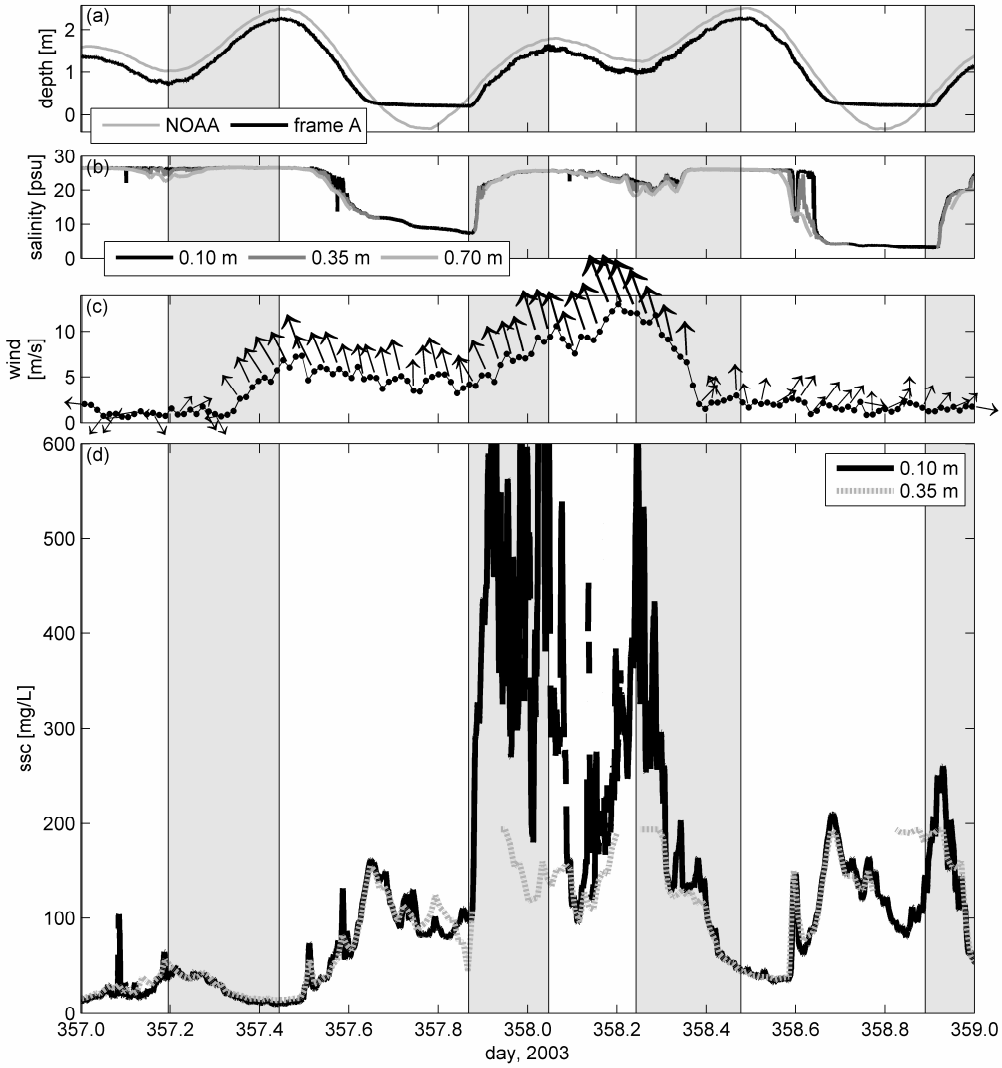

Figure 7. Conditions in mudflat channel during winds from the south. (a) Water surface in the channel, tidal stage, and precipitation; (b) salinity 0.10 m, 0.35 m, and 0.70 m above the bed; (c) wind speed and direction; (d) suspended sediment concentration 0.10 m and 0.35 m above the bed.

Figure 8

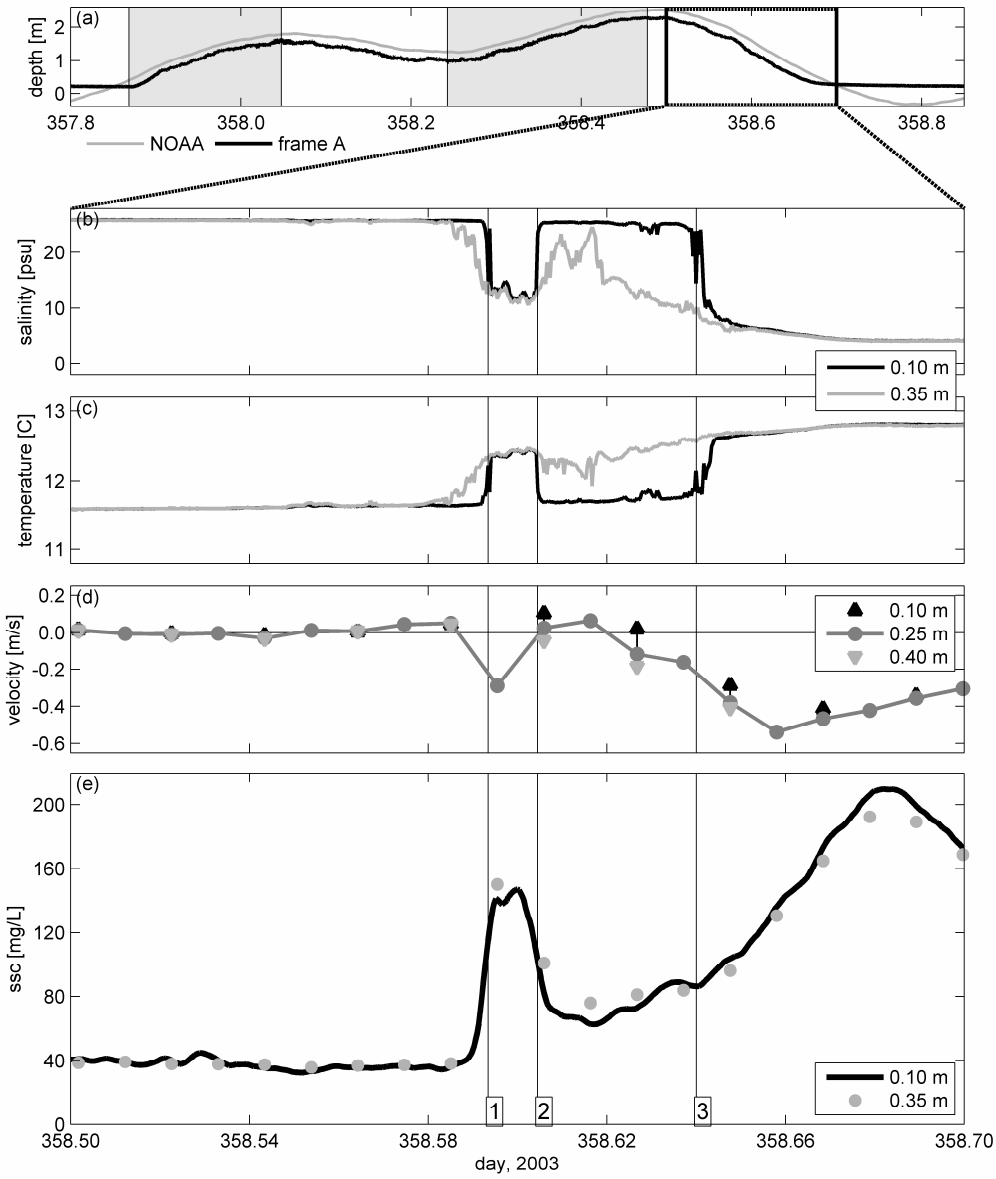

Figure 8. Conditions in mudflat channel after moderate precipitation. (a) Depth and tidal stage for the entire inundation, with the period in the lower panels highlighted. (b) Salinity 0.10 m, and 0.35 m above the bed; (c) temperature 0.10 m, and 0.35 m above the bed; (d) along-channel velocity 0.10 m, 0.25 m, and 0.40 m above the bed; (c) suspended sediment 0.10 m and 0.35 m above the bed.

Figure 9

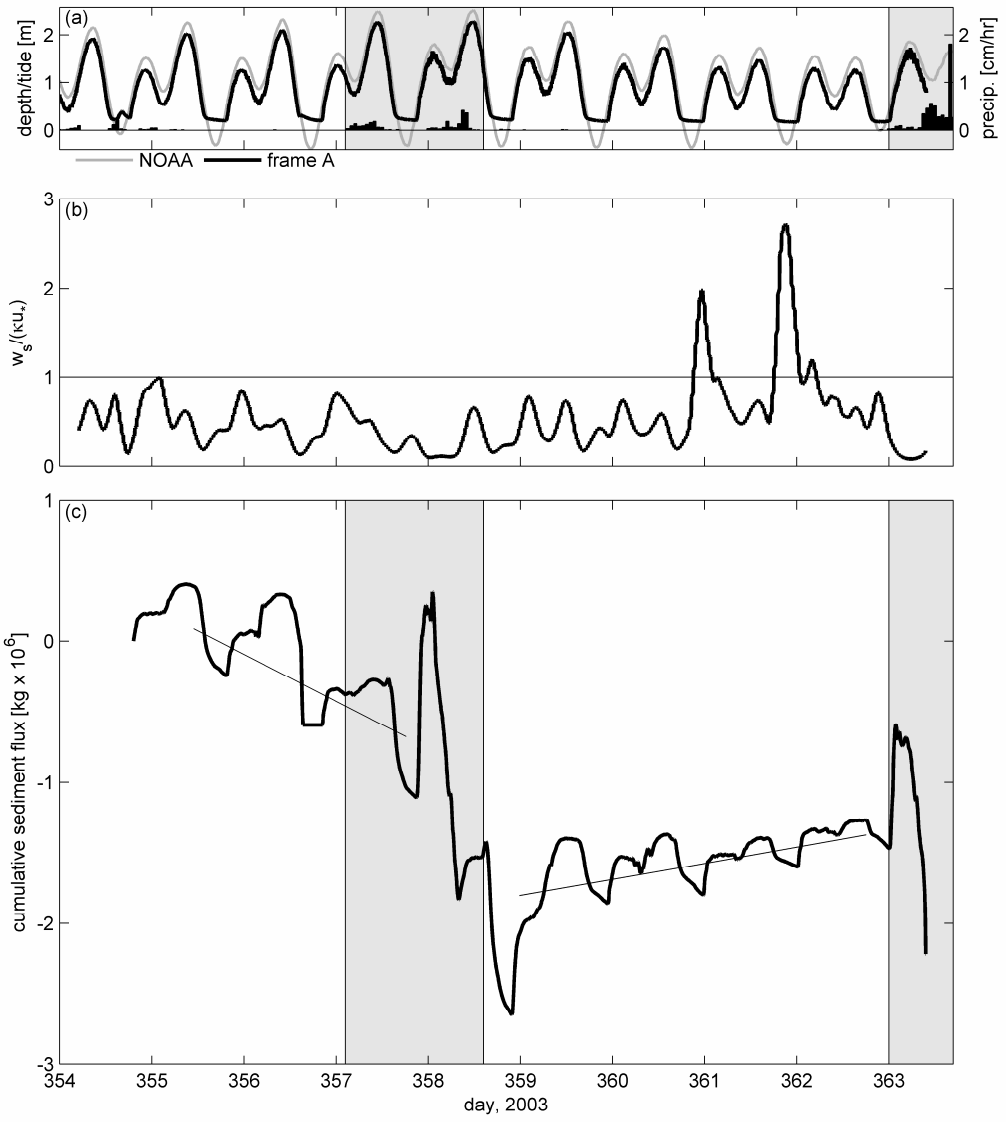

Figure 9. Rouse number and cumulative sediment flux. (a) Water surface, tidal stage, and precipitation, with periods of precipitation highlighted gray; (b) Rouse number, $P = w_s/(\kappa u_*)$; (c) cumulative sediment flux in the channel from the beginning of the deployment, with positive slope for onshore transport and negative slope for offshore transport.